A Dual-Function Massive MIMO Uplink OFDM Radar Communication Architecture

Murat Temiz, *Member, IEEE*, Emad Alsusa, *Senior Member, IEEE,* and Mohammed W. Baidas, *Senior Member, IEEE*

***Abstract*—This paper proposes a joint uplink massive multiple-input-multiple-output (MIMO) communication and orthogonal frequency-division multiplexing (OFDM) radar sensing architecture. Specifically, uplink communication and short-range radar sensing are considered, where the user equipments (UEs) transmit data to the base-station (BS), which simultaneously receives radar returns from the targets over the same subcarriers. Hence, the signals received at each BS antenna include radar returns and communication signals to be processed for extracting the sensing and communication data. The separation and detection of such signals are achieved by utilizing the channel diversity between the UEs and the targets. To this end, the UEs' signals are first detected and demodulated, and then subtracted from the received signal to acquire the radar returns. Symbol-based radar processing is then employed, as it provides substantial processing gains, and its detection performance is independent of the transmitted radar waveform. Furthermore, self-interference—due to the simultaneous operation of transmit and receive antennas—is taken into account. The communication capacity and normalized error of the radar-target channel estimation are mathematically analyzed, and the trade-off between the communication capacity and radar detection performance is demonstrated in terms of the power output of the communication and radar sub-systems, as well as the signal-to-noise ratio.**

***Index Terms*—Interference cancellation, massive MIMO, radar-communication architecture, 6G networks**

I. Introduction

The growing number of connected mobile devices and their service requirements have pushed the mobile communication networks to support additional functions and services. For instance, while previous generations of networks were mainly designed and standardized to provide mobile broadband Internet and voice services, 5G has been developed to comprehensively support massive machine-type communication (mMTC), machine-to-machine (M2M) communication, massive Internet-of-Things, (mIoT) and ultra-reliable and low-latency communication (URLLC), in addition to enhanced mobile broadband (eMBB) [1,2]. Additionally, radio sensing technologies are becoming an integral part of some commercial and industrial applications (e.g. autonomous driving and intelligent transportation systems), especially with the recent advancements in artificial intelligence and machine learning techniques, with the goal of sensing the surroundings for safe and intelligent driving [3,4]. There are also other possible applications of radar sensing, such as detection of drones [5]–[7], and factory automation [8]. Such applications also require a reliable communication infrastructure to safely and seamlessly operate, and hence, are expected to be incorporated into mobile networks [9,10]. Consequently, 5G and beyond mobile network architectures are envisaged to provide communication as well as radar sensing capabilities, especially for smart vehicles, unmanned aerial vehicles (UAVs), localization, and industrial automation applications [4,11,12]. Thus, several studies have proposed various methods to enable dual-function radar and communication (RadCom) platforms using the same time-frequency resources on the same platform. Specifically, radar sensing and communication may be jointly performed by the base-station (BS) using the same hardware to efficiently utilize the scarce frequency resources and improve the energy-efficiency of the system [10,13,14]. While the joint transmission of a radar waveform along with downlink communication (or transmitting an integrated waveform) has extensively been investigated recently with various techniques being proposed for such purposes [15]–[20], jointly receiving radar returns and uplink communication signals is still very much the subject of attention and extensive research. For instance, a pulsed long-range radar with downlink and uplink communication is considered in [9], where the radar returns are estimated from the received signals during uplink by assuming that the radar returns are always received earlier than the uplink communication signals. Based on this assumption, the radar returns are estimated during the guard time, and the partially overlapping radar returns with the uplink communication data are estimated and subtracted from the received signals to acquire the communication data. In a different approach, proposed in [21], the transmitted signals by the UEs are utilized for sensing during uplink. These signals are reflected by the targets and captured by the BS to estimate the target parameters. However, this uplink sensing model has limited capabilities, since the signals' delay is related to the distance of the UEs, which is unknown, and the power output of the UEs is limited. Another study utilizes two transceivers with steerable analogue antenna arrays to jointly perform radar sensing and communication during uplink and downlink [20]. On the other hand, interference from radars on uplink massive MIMO is investigated in [22], where the authors consider a long-range radar that transmits its waveforms while a massive MIMO BS receives uplink signals from its UEs at the same frequency. Under this assumption, the communication capacity was analyzed; however, the radar detection performance was not considered, since the study was mainly focused on the

M. Temiz and E. Alsusa are with the Department of Electrical and Electronic Engineering, University of Manchester, Manchester, UK and M. W. Baidas is with the Department of Electrical Engineering, Kuwait University, Kuwait. (e-mail: {murat.temiz, e.alsusa}@manchester.ac.uk, m.baidas@ku.edu.kw)

impact of the radar interference on the massive MIMO uplink.

In contrast to the existing literature, this work proposes a different approach to perform uplink sensing and satisfy certain radar detection performance and communication data-rate requirements. Particularly, a large-scale antenna array is employed along with radar transmit antennas. The spatial diversity between the UEs and targets is exploited to suppress radar returns and estimate the communication data. Subsequently, the estimated communication data is subtracted from the received signals to acquire the radar returns. Notably, a receiver design for joint communication and short-range sensing also needs to alleviate (or even eliminate) the self-interference between the transmit and receive antennas, in addition to separating the communication data and radar returns, which is considered in this work. It is worth noting that joint massive MIMO OFDM downlink communication and radar sensing was investigated in [14], where interference exploitation based precoder schemes were proposed to improve communication capacity and radar detection. Thus, this study focuses only on simultaneous uplink communication and radar sensing using the same hardware. The main contributions of this work can be summarized as follows:

- Propose a dual-function radar-communication (RadCom) system, which employs large-scale antenna arrays to communicate with multiple uplink UEs, while sensing the targets in range.
- Derive analytical capacity expressions for the proposed RadCom system with perfect and imperfect channel state information (CSI), and evaluate its communication capacity and radar detection performance under various operational conditions.

In the rest of the paper, Section II presents the system model, while Section III discusses the communication signal detection and radar target estimation methods. In Section IV, the analytical communication capacity expressions are derived, whereas Section V validates the derived analytical capacity expressions, and evaluates the communication capacity and radar detection performance. Finally, Section VI draws the conclusions.

Notation: Throughout the paper, the following notation is used. Bold uppercase letters (e.g. $\mathbf{H}$) indicate matrices, while bold lowercase letters (e.g. $\mathbf{h}$) indicate vectors. Superscripts * and ^{H} indicate the conjugate and Hermitian transpose, respectively. The expectation, absolute value, and Euclidean norm operators are denoted by $\mathbb{E}[.]$, $|.|$, and $\|.\|$, respectively.

II. System Model

In this study, multiple uplink UEs communicate with the massive MIMO BS which simultaneously performs radar sensing using the overlapping subcarriers with the uplink communication. The BS antenna array consists of M antennas for receiving communication and radar signals, and $Q = 2$ radar transmit antennas that transmit OFDM radar waveforms[1]. The orthogonality between the transmitted radar waveforms is ensured by transmitting interleaved OFDM radar waveforms [23]. Therefore, over each subcarrier, only one radar transmit antenna actively transmits, and all available subcarriers are equally shared by the radar transmit antennas in an interleaved manner. Synchronized time division duplexing (TDD) is selected as the operation mode of the network, since uplink channel estimation is sufficient for the UEs data communication within the coherence time. Since vehicular networks are targeted, a short-range radar with up to $R_{max} = 200$ m range is considered for the sensing, and the maximum round-trip time of the radar waves is $\tau_{r,max} = 2R_{max}/c_0 = 1.33$ μs within this radar range, where c_0 is the speed of light. This is a very short duration compared to the duration of TDD downlink and uplink subframes. Thus, the radar transmit antenna must remain continuously operational for sensing during uplink. A TDD frame includes channel estimation (CE), and downlink and uplink subframes, as shown in Fig. 1. During channel estimation, all BS antennas receive the pilot symbols transmitted by the UEs, and the BS estimates the CSI between the antennas and the UEs.

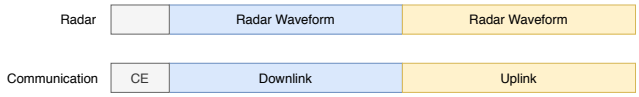

(b)

Fig. 1. Synchronized TDD frame for data communication and radar sensing.

A. Radar and Communication Signal Models

During uplink transmission, the two radar transmit antennas omnidirectionally emit orthogonal and interleaved radar waveforms over L subcarriers, while the UEs transmit their data signals to the BS. Thus, the BS antenna array elements receive the sum of the transmitted signals by the UEs and the radar returns from the targets. Let $\mathbf{S}_q \in \mathbb{C}^{N\times L/2}$ denote the transmitted baseband OFDM radar waveform by the qth radar antenna (for $q \in \{1, 2\}$), which consists of N phase-shift keying (PSK) symbols over $L/2$ subcarriers, as

$$\mathbf{S}_q = \begin{pmatrix} s_{1,q} & s_{1,q+2} & \cdots & s_{1,q+L-2} \\ s_{2,q} & s_{2,q+2} & \cdots & s_{2,q+L-2} \\ \vdots & \vdots & \ddots & \vdots \\ s_{N,q} & s_{N,q+2} & \cdots & s_{N,q+L-2} \end{pmatrix}. \quad (1)$$

Furthermore, for the sake of simplicity, $s_{\mu,l}$ denotes the μth PSK radar symbol in the lth subcarrier, where $\mu \in \{1, 2, \ldots, N\}$ and $l \in \{1, 2, \ldots, L\}$. On the other hand, the transmitted baseband quadrature-amplitude modulation (QAM) symbols in the lth subcarrier by K UEs are expressed as vector $\mathbf{x}_l = [x_1, \ldots x_k, \ldots, x_K]^T \in \mathbb{C}^{K\times 1}$.

B. Communication Channel Model

Let the channel matrix between the K UEs and M BS antennas be denoted $\mathbf{H} \in \mathbb{C}^{M\times K}$, and each entry is given by $h_{m,k} = \beta_k f_{m,k}$, where β_k is the large-scale fading of the kth UE, while $f_{m,k}$ is the small-scale fading between the mth antenna and the kth UE. Moreover, $f_{m,k}$ follows a zero-mean

[1]Note that it is possible to employ more than two radar transmit antennas to simultaneously transmit orthogonal OFDM waveforms in an interleaved way for MIMO radar sensing [23]; however, for the sake of simplicity, only two radar transmit antennas are considered in this work.

complex Gaussian distribution with unit variance, as $f_{m,k} \sim \mathcal{CN}(0,1)$. The large-scale fading of the kth UE is calculated as $\beta_k = 10^{-PL_k/10}$, where

$$PL_k = 10\log_{10}\left(\frac{4\pi f_c d_0}{c_0}\right)^2 + 10\log_{10}\left(\frac{d_k}{d_0}\right)^{\varphi} + \zeta_{sh}, \quad (2)$$

in which f_c, d_0, and φ are the carrier frequency, reference distance, and the path-loss exponent, respectively. Moreover, $30 \leq d_k \leq 400$ is the distance of the kth UE to the BS, and ζ_{sh} is the log-normal shadow fading, distributed as a zero-mean Gaussian random variable with standard deviation σ_{sh}. These parameters are determined based on the non-line-of-sight (NLOS) urban macrocell measurements detailed in [24], as $f_c = 5.8$ GHz, $d_0 = 1$ m, $\varphi = 2.9$, and $\sigma_{sh} = 5.7$ dB.

The CSI of the UEs is acquired during uplink channel estimation by exploiting the pilot symbols transmitted by UEs. For channel estimation, LS and MMSE estimators are commonly employed due to their low-complexity and sufficient estimation accuracy. Various parameters, such as thermal noise, RF chain non-linearities and pilot contamination, may degrade the CSI estimation accuracy, and thus, a generic CSI error model is employed in this study [25]. Let ξ be the variance of channel estimation errors, which can be modeled as $\xi = a\rho^{-b}$, where ρ is the UE received signal-to-noise ratio (SNR), and a and b are error parameters [26]. Based on this error model, the estimated channel vector of the kth UE—including estimation errors—is given by

$$\hat{\mathbf{h}}_k = \sqrt{1-\xi}\mathbf{h}_k + \mathbf{e}_k, \quad (3)$$

where $\mathbf{e}_k \in \mathbb{C}^{M\times 1}$ denotes the error vector and its entries follow a zero-mean complex Gaussian distribution as $e_{m,k} \sim \mathcal{CN}(0, \xi\beta_k)$. In turn, $\mathbb{E}\left[|e_{m,k}|^2\right] = \xi\beta_k$, and hence, $\mathbb{E}\left[|h_{m,k}|^2\right] = \mathbb{E}\left[\left|\hat{h}_{m,k}\right|^2\right] = \beta_k$, which ensures that imperfectly estimated channels have the same average channel gains as the real channels. Note that $\xi = 0$ corresponds to the perfectly estimated CSI, while $\xi = 1$ implies that the estimated channel is entirely independent of the channel matrix.

C. Radar Channel Model

Although communication channels are generally modeled as NLOS, channels between the radar and targets usually have a predominant LOS component and are modeled as two-way channels, since the signals transmitted by the radar are reflected off the target, and then received by the receive antennas. Assuming U targets are present in the range, the channel between the qth radar transmit antenna, U targets, and mth receive antenna over the lth subcarrier, is modeled as [27]

$$g_{m,q} = \sum_{u=1}^{U} a_{u,m,q} e^{-j2\pi l\Delta f\Theta_u} e^{j2\pi f_{D,u}\mu t_o}, \quad (4)$$

where $e^{-j2\pi l\Delta f\Theta_u}$ with $\Theta_u = (R_{u,q} + R_{u,m})/c_0$ is the phase shift owing to the total path length $(R_{u,q}+R_{u,m})$ from the qth radar transmit antenna to the target $R_{u,q}$, and from the target to the mth antenna element $R_{u,m}$. Moreover, l and Δf denote the subcarrier index and OFDM subcarrier spacing, respectively [27]. The second phase shift term—given by $e^{j2\pi f_{D,u}\mu t_o}$—includes velocity information of the targets, where t_o denotes the duration of an OFDM symbol. The Doppler shift caused by the target velocity is given by $f_{D,u} = 2v_u f_c/c_0$, where v_u denotes relative speed of the uth target. According to radar equation in [28], the gain of the two-way channel between the radar transmit antenna, the uth target and the qth radar receive antenna is given by

$$a_{u,m,q} = \frac{\lambda\sqrt{G_q G_m \sigma_u}}{(4\pi)^{3/2} R_{u,tx} R_{u,m}}, \quad (5)$$

where G_q and G_m denote the the transmit and receive antenna gains, respectively. Moreover, σ_u is the radar cross-section (RCS) of the target. Consequently, the radar channel vector between the qth radar transmit antenna, U targets, and M receive antennas is given by

$$\mathbf{g} = [g_{1,q}\ g_{2,q}\ \cdots\ g_{M,q}]^T \in \mathbb{C}^{M\times 1}. \quad (6)$$

D. Direct-Coupling Channel Model

Since the radar transmit antennas operate at the same time as the M receive antennas for data communication and radar returns, direct-coupling occurs between the closely located transmit and receive antennas. An adequately designed antenna array can provide 80 dB antenna isolation [29], and this is sufficient to prevent the receive antennas saturation and protect their RF chains. The direct-coupling channel is relatively deterministic compared to the radar and communication channels, as the antennas are fixed in the array [30]. The direct-coupling channel vector between a single radar transmit and M receive antennas over the lth subcarrier is denoted by $\mathbf{c}_l \in \mathbb{C}^{M\times 1}$. Each entry of the direct-coupling vector is modeled as $c_{m,q} = \Lambda_{m,q} e^{-2\pi j d_{m,q}/\lambda}$ [31], where $\Lambda_{m,q}$ is the channel gain of the direct-coupling, and $d_{m,q}$ is the distance between the qth radar transmit and the mth receive antenna and $j = \sqrt{-1}$. The direct-coupling channel gain with a satisfactory isolation between the antennas was measured as $\Lambda_{m,q}[\text{dB}] = -70$ dB [5]. The direct-coupling channel vector can be estimated, and the radar can be calibrated to cancel out or mitigate the self-interference, since the transmitted radar waveform and the coupling channels are known by the BS [32,33].

E. Received Signal Model

The received signal at the BS over the lth subcarrier during the tth sampling time is given by

$$\begin{aligned}\mathbf{y}_l(t) = &\sqrt{p_u}\mathbf{H}_l(t)\,\mathbf{x}_l(t-\tau_c) + \sqrt{p_{rad}}\mathbf{c}_l(t)\,s_{\mu,l}(t)\\ &+ \sqrt{p_{rad}}\mathbf{g}_l(t)\,s_{\mu,l}(t-\tau_r) + \mathbf{n}_l, \end{aligned} \quad (7)$$

where τ_c and τ_r are the delays of the communication signals and radar returns, respectively. Moreover, $\mathbf{H}_l$, $\mathbf{g}_l$ and $\mathbf{n}_l$ denote the communication channel matrix, radar channel vector and noise vector received over the lth subcarrier, respectively. Each entry of $\mathbf{n}_l$ follows a Gaussian distribution with mean 0 and standard deviation σ_n^2, i.e., $n \sim \mathcal{CN}\left(0, \sigma_n^2\right)$. Furthermore, p_u

is the transmit power of each UE as the total UE transmit power is given $p_{com} = Kp_u$, and p_{rad} is the transmit power of a single radar antenna. Since the transmit and receive antennas are very close to each other, the delay of the self-interference signal is omitted. The cyclic-prefix (CP) duration T_{cp} of the OFDM signals is set to the maximum delay of the radar returns. Assuming that the maximum range of the radar is $R_{max} = 200$ m, then $T_{cp} = \tau_{r,max} = 1.33$ μs. Since the OFDM symbol duration is much longer than the maximum delay of radar returns and delay spread of communication signals, then the delay of the signals in each sampling time can be omitted. Moreover, t and l can be dropped from (7) for the sake of simplicity. Accordingly, the sampled received baseband signal at the BS can be expressed as

$$\mathbf{y} = \sqrt{p_u}\mathbf{H}\mathbf{x} + \sqrt{p_{rad}}\mathbf{c}s_\mu + \sqrt{p_{rad}}\mathbf{g}s_\mu + \mathbf{n}. \tag{8}$$

III. Communication Signal Detection and Radar Target Estimation

This section presents the communication signal detection and radar target estimation from the received signals. Firstly, the self-interference (SI) is canceled or mitigated by subtracting the product of the transmitted radar signal and the estimated direct-coupling channel from the received signals over each subcarrier, as shown in Fig. 2. After that, communication symbol detection and the radar target estimation are consecutively performed. In the following subsections, self-interference cancellation, communication data detection, and radar target estimation are detailed.

A. Self-Interference Cancellation

In the received signal vector $\mathbf{y}$, the direct-coupling vector is estimated and self-interfering radar signals are removed by the digital SI canceller before the signal detection is performed. Let $\hat{\mathbf{c}}_l \in \mathbb{C}^{M\times 1}$ denote the estimated direct-coupling vector for M antennas in the lth subcarrier from a single active transmit antenna. Then, the residual SI after cancellation is given by

$$\mathbf{y}_{SI} = (\mathbf{c}_l - \hat{\mathbf{c}}_l)\sqrt{p_{rad}}s_\mu. \tag{9}$$

If the direct-coupling vector is estimated entirely correct (i.e. $\mathbf{c}_l = \hat{\mathbf{c}}_l$), then SI will be completely cancelled (i.e. $\mathbf{y}_{SI} = \mathbf{0}$). However, the estimation of the direct-coupling vector may include amplitude or phase estimation errors, and this leads to residual SI. In this case, the residual SI is modeled as

$$\mathbf{y}_{SI} = (\mathbf{c}_l - \hat{\mathbf{c}}_l)\sqrt{p_{rad}}s_\mu = \sqrt{\gamma_{SI}}\sqrt{p_{rad}}\mathbf{c}_l s_\mu, \tag{10}$$

where γ_{SI} denotes the SI suppression error after the digital canceller. For instance, in the case of perfect SI cancellation, $\gamma_{SI} = 0$. For the sake of simplicity, considering that direct-coupling channel is estimated with an average error for M antennas, then the relation between the direct-coupling channel coefficients c_m, and their estimations $\hat{c}_m$ (for $m = 1, 2, \ldots, M$) is expressed as

$$\frac{1}{M}\sum_{m=1}^{M}\hat{c}_m = \frac{1}{M}\sum_{m=1}^{M}\left(c_m - \sqrt{\gamma_{SI}}c_m\right). \tag{11}$$

Consequently, the estimated channel coefficient for the mth antenna is given by

$$\hat{c}_m = c_m - \sqrt{\gamma_{SI}}c_m. \tag{12}$$

Hence, the SI suppression error can be expressed as

$$\sqrt{\gamma_{SI}} = \left|\frac{r_m e^{j\alpha_m} - \hat{r}_m e^{j\hat{\alpha}_m}}{r_m e^{j\alpha_m}}\right|, \tag{13}$$

where r_m and $\hat{r}_m$ denote the amplitude of the direct-coupling and estimated direct-coupling coefficients c_m and $\hat{c}_m$, respectively. Moreover, α_m and $\hat{\alpha}_m$ denote their phases, respectively (i.e. $c_m = r_m e^{j\alpha_m}$ and $\hat{c}_m = \hat{r}_m e^{j\hat{\alpha}_m}$). Therefore, the SI suppression error is given by

$$\gamma_{SI} = \left|1 - \frac{\hat{r}_m}{r_m}e^{j(\hat{\alpha}_m - \alpha_m)}\right|^2, \tag{14}$$

which indicates that this SI suppression error model considers both amplitude and phase SI estimation errors.

A linear SI cancellation technique was reported to achieve -40 dB SI attenuation in [29], while non-linear SI cancellation techniques were reported to achieve -45 dB SI attenuation in [29], and -48 dB SI attenuation in [33]. Considering a satisfactory antenna isolation [5,29] and digital SI cancellation [33], the total SI suppression can reach around $\gamma_{SI} = -130$ dB in a well-designed system, and this can be improved by further isolating the transmit and receive antennas. Moreover, the residual SI in the radar image is usually observed as a static object very close to the radar, and hence, it can be recognized and eliminated during radar image processing [34]. Consequently, the residual SI is expected to degrade only the capacity of the communication, as it can already be detected and eliminated in the radar image.

B. Communication Signal Detection

After cancelling or mitigating the SI, the rest of the signal is processed to separate communication and radar signals. Having a large-scale antenna array, the radar interference arriving at the BS through unknown channels can be suppressed, since the communication channel matrix is estimated, and hence is entirely or partially known. Although the maximum-likelihood (ML) receiver is the optimum detector for MIMO systems, its complexity exponentially increases with the number of UEs and constellation size of the modulation scheme [35]. Therefore, the zero-forcing (ZF), and the ZF with ordered successive interference cancellation (ZF-OSIC) receivers are considered in this study. While the ZF is a linear receiver, the ZF-OSIC is a non-linear receiver, which iteratively operates to maximize the multiplexing gain.

The ZF receiver, denoted $\mathbf{W}_{ZF} \in \mathbb{C}^{K\times M}$, is given by [36]

$$\mathbf{W}_{ZF} = \left(\hat{\mathbf{H}}_{com}^H \hat{\mathbf{H}}_{com}\right)^{-1}\hat{\mathbf{H}}_{com}^H, \tag{15}$$

which is also equal to the pseudo-inverse of the estimated channel matrix $\hat{\mathbf{H}}$. The acquired signal from the UEs using the ZF receiver is given by

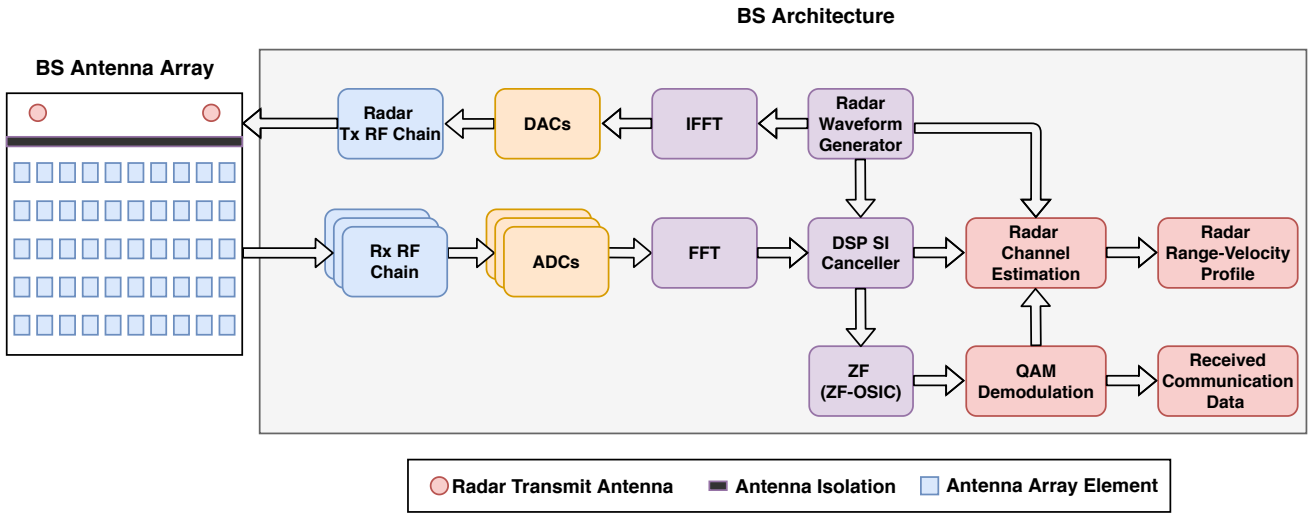

Fig. 2. Uplink massive MIMO OFDM RadCom BS Architecture.

$$\begin{aligned}\hat{\mathbf{x}} &= \mathbf{W}_{ZF}\mathbf{y} \\ &= \sqrt{p_u}\mathbf{W}_{ZF}\mathbf{H}\mathbf{x} + \mathbf{W}_{ZF}\sqrt{\gamma_{SI}p_{rad}}\mathbf{c}s_\mu \\ &+ \mathbf{W}_{ZF}\sqrt{p_{rad}}\mathbf{g}s_\mu + \mathbf{W}_{ZF}\mathbf{n}. \end{aligned} \tag{16}$$

On the other hand, when the ZF-OSIC is employed, the symbol transmitted by the UE with the best channel condition is firstly detected, and after removing its symbols from the received signals, the UE with the second best channel condition is detected and so on. To this end, the estimated channel vectors of the K UEs are ordered and detected with respect to their norms, as $\left\|\hat{\mathbf{h}}_1\right\| \geq \left\|\hat{\mathbf{h}}_2\right\| \geq \cdots \geq \left\|\hat{\mathbf{h}}_K\right\|$. This ensures that the earlier detected symbols have a higher probability of correct detection, as they would affect the detection of the subsequent symbols. The symbol of the kth UE is estimated by ZF-OSIC as [37]

$$\widetilde{x}_k = \widetilde{\mathbf{w}}_k\widetilde{\mathbf{y}}_k, \tag{17}$$

where the residual signal vector $\widetilde{\mathbf{y}}_k$—after removing the symbol of the kth UE—is given by

$$\widetilde{\mathbf{y}}_k = \mathbf{y} - \sqrt{p_u}\sum_{i=1}^{k-1}\mathbf{h}_i\widetilde{x}_i, \tag{18}$$

and the ZF precoder for the kth UE is given by

$$\widetilde{\mathbf{w}}_k = \left[\left(\hat{\mathbf{H}}_k^H\hat{\mathbf{H}}_k\right)^{-1}\hat{\mathbf{H}}_k^H\right]_{1,:}, \tag{19}$$

where $[.]_{1,:}$ denotes the first row the parameter matrix. The channel matrix for the rest of the UEs is given

$$\hat{\mathbf{H}}_k = \left[\hat{\mathbf{h}}_k, \hat{\mathbf{h}}_{k+1}, \cdots, \hat{\mathbf{h}}_K\right]. \tag{20}$$

After the ZF or ZF-OSIC processes, the detected symbol vector $\widetilde{\mathbf{x}} = [\widetilde{x}_1, \widetilde{x}_2, \ldots, \widetilde{x}_K]$ of the UEs is obtained.

C. Radar Signal Estimation

After detecting all symbols transmitted by the UEs via either ZF or ZF-OSIC, the baseband radar signal vector, $\mathbf{r} \in \mathbb{C}^{M\times 1}$, can be obtained—by subtracting the product of the detected symbols and the estimated channel vectors from the received signal vector—as

$$\begin{aligned}\mathbf{r} &= \mathbf{y} - \sqrt{p_u}\sum_{k=1}^{K}\hat{\mathbf{h}}_k\widetilde{x}_k. \\ &= \sqrt{p_u}\mathbf{H}\mathbf{x} - \sqrt{p_u}\hat{\mathbf{H}}\widetilde{\mathbf{x}} + \sqrt{p_{rad}}\left(\sqrt{\gamma_{SI}}\mathbf{c} + \mathbf{g}\right)s_\mu + \mathbf{n}, \end{aligned} \tag{21}$$

in which $\mathbf{r}$ consists of the radar signals received by M antennas after removing the communication data. For velocity and range estimation of the targets, the signals received by only one antenna is sufficient; however, by combining the received signals by all antennas, the detection accuracy can be improved. For the sake of simplicity, only one receive antenna for radar detection is considered in this work. Let $r_{m,l}$ denote the recovered radar signal from the mth antenna over the lth subcarrier. Then, the radar channel is estimated by element-wise division of the estimated radar vector $\mathbf{r}$ by the transmitted radar symbol $s_{\mu,l}$ as [38]

$$\hat{g}_{m,\mu,l} = \frac{r_{m,l}}{\sqrt{p_{rad}}s_{\mu,l}} = \frac{\left[\mathbf{y} - \hat{\mathbf{H}}\widetilde{\mathbf{x}}\right]_m}{\sqrt{p_{rad}}s_{\mu,l}}, \tag{22}$$

where $[\cdot]_m$ denotes the mth entry of the parameter vector. By substituting (8) and (10) into (22), the estimated radar channel is obtained as

$$\hat{g}_{m,\mu,l} = g_{m,u,l} + \underbrace{\left[\frac{\sqrt{p_u}\left(\mathbf{H}\mathbf{x} - \hat{\mathbf{H}}\widetilde{\mathbf{x}}\right) + \sqrt{\gamma_{SI}p_{rad}}\mathbf{c}s_{\mu,l} + \mathbf{n}}{\sqrt{p_{rad}}s_{\mu,l}}\right]_m}_{interference+noise}, \tag{23}$$

where the residual communication interference, residual SI and noise are observed to deteriorate the radar estimation

performance. By rearranging all estimated channel coefficients into an $N \times L$ matrix, the estimated radar channel matrix consisting of N symbols over L subcarriers of the mth receive antenna is obtained as

$$\hat{\mathbf{G}}_m = \begin{pmatrix} \hat{g}_{m,1,1} & \hat{g}_{m,1,2} & \cdots & \hat{g}_{m,1,L} \\ \hat{g}_{m,2,1} & \hat{g}_{m,2,2} & \cdots & \hat{g}_{m,2,L} \\ \vdots & \vdots & \ddots & \vdots \\ \hat{g}_{m,N,1} & \hat{g}_{m,N,2} & \cdots & \hat{g}_{m,N,L} \end{pmatrix}. \tag{24}$$

The symbol-based radar processing is employed to estimate the range and velocity of the targets. This radar processing is performed by taking the DFT/IDFT of the channel radar matrix $\hat{\mathbf{G}}_m$ [27,38]. Specifically, taking IDFT of the radar channel matrix $\hat{\mathbf{G}}_m$ along the frequency axis results in range profile, while the DFT along the symbol axis gives the velocity profile [38]. Accordingly, the radar-range profile matrix is given by

$$\mathbf{P}_m = \mathrm{DFT}_\mu \left[\mathrm{IDFT}_l \left[\hat{\mathbf{G}}_m \right] \right], \tag{25}$$

which will have maximum values at the estimated targets range and velocity points. Moreover, this symbol-based radar processing provides a processing gain of $G_p = N \times L$ for each receive antenna. The signal-to-interference-plus-noise ratio (SINR) of the radar image ψ_{rad} is computed by ignoring the direct-coupling—since it can be recognized and removed during the radar image—as

$$\psi_{rad} = \frac{G_p p_{rad} \left\| \mathbf{g} \right\|^2}{p_u \left\| \mathbf{H}\mathbf{x} - \hat{\mathbf{H}}\widetilde{\mathbf{x}} \right\|^2 + \left\| \mathbf{n} \right\|^2}, \tag{26}$$

which indicates that if the BS has the perfect CSI and estimates the communication symbols correctly (i.e. $p_u \left\| \mathbf{H}\mathbf{x} - \hat{\mathbf{H}}\widetilde{\mathbf{x}} \right\|^2 = 0$), the radar achieves the maximum detection performance. Contrarily, the radar detection will be affected by the imperfectly estimated communication CSI and wrongly detected symbols. The radar channel estimation error after canceling the communication signal is given by

$$\begin{aligned} \mathbf{e}_{rad} &= \mathbf{g} - \frac{\left(\sqrt{p_u} \left(\mathbf{H}\mathbf{x} - \hat{\mathbf{H}}\widetilde{\mathbf{x}} \right) + \sqrt{p_{rad}} \mathbf{g} s_\mu + \mathbf{n} \right)}{\sqrt{p_{rad}} s_\mu} \\ &= \frac{\sqrt{p_u} \left(\mathbf{H}\mathbf{x} - \hat{\mathbf{H}}\widetilde{\mathbf{x}} \right) + \mathbf{n}}{\sqrt{p_{rad}} s_\mu}. \end{aligned} \tag{27}$$

Furthermore, the normalized error of the radar-target channel estimation is given by

$$\phi_{rad} \triangleq \frac{\left\| \mathbf{e}_{rad} \right\|^2}{\left\| \mathbf{g} \right\|^2} = \frac{p_u \left\| \left(\mathbf{H}\mathbf{x} - \hat{\mathbf{H}}\widetilde{\mathbf{x}} \right) \right\|^2 + M\sigma_n^2}{p_{rad} \left\| \mathbf{g} \right\|^2}, \tag{28}$$

since $\left| s_\mu \right|^2 = 1$, $\left\| \mathbf{n} \right\|^2 = M\sigma_n^2$ and $\mathbf{H}$ and $\mathbf{n}$ are mutually independent.

IV. Capacity Analysis

In this section, analytical communication capacity expressions are derived by taking into account channel estimation errors, residual SI, and radar interference. Recall that M BS antennas receive the signal vector, which consists of uplink data of UEs, the radar signals reflected off the targets, and the self-interference from the radar transmit antenna. Moreover, ZF and ZF-OSIC receivers can cancel out the inter-user interference when the perfect CSI is available at the BS. Also, the ZF-OSIC receiver further suppresses the noise and radar interference. In turn, the capacity expression of the ZF receiver is firstly derived and then the extra noise and interference suppression gained by ZF-OSIC is incorporated to obtain the capacity expression of the ZF-OSIC.

The received signal vector $\mathbf{y} \in \mathbb{C}^{M \times 1}$ after SI cancellation is given by

$$\mathbf{y} = \sum_{k=1}^{K} \sqrt{p_u} \mathbf{h}_k x_k + \sqrt{\gamma_{SI} p_{rad}} \mathbf{c} s_\mu + \sqrt{p_{rad}} \mathbf{g} s_\mu + \mathbf{n}. \tag{29}$$

After the ZF processing, the following signal is obtained,

$$\begin{aligned} \hat{\mathbf{x}} &= \mathbf{W}_{ZF} \mathbf{y} \\ &= \mathbf{W}_{ZF} \sum_{k=1}^{K} \sqrt{p_u} \mathbf{h}_k x_k + \mathbf{W}_{ZF} \sqrt{\gamma_{SI} p_{rad}} \mathbf{c} s_\mu \\ &\quad + \mathbf{W}_{ZF} \sqrt{p_{rad}} \mathbf{g} s_\mu + \mathbf{W}_{ZF} \mathbf{n}, \end{aligned} \tag{30}$$

and the received signal from the kth UE can explicitly be written as

$$\begin{aligned} \hat{x}_k = &\underbrace{\sqrt{p_u} \mathbf{w}_k \mathbf{h}_k x_k}_{desired\ signal} + \underbrace{\sum_{i=1, i \neq k}^{K} \sqrt{p_u} \mathbf{w}_k \mathbf{h}_i x_i}_{inter-user\ interference} \\ &+ \underbrace{\mathbf{w}_k \left(\sqrt{\gamma_{SI} p_{rad}} \mathbf{c} s_\mu + \sqrt{p_{rad}} \mathbf{g} s_\mu + \mathbf{n} \right)}_{SI+radar\ interference+noise}. \end{aligned} \tag{31}$$

By substituting the channel error model given by (3) into (31), the detected signal $\hat{x}_k$ from the kth UE with imperfect CSI estimation is obtained as

$$\begin{aligned} \hat{x}_k = &\sqrt{p_u} \left(\frac{\mathbf{w}_k \hat{\mathbf{h}}_k - \mathbf{w}_k \mathbf{e}_k}{\sqrt{1-\xi}} \right) x_k \\ &+ \sum_{i=1, i \neq k}^{K} \sqrt{p_u} \left(\frac{\mathbf{w}_k \hat{\mathbf{h}}_i - \mathbf{w}_k \mathbf{e}_i}{\sqrt{1-\xi}} \right) x_i \\ &+ \mathbf{w}_k \left(\sqrt{\gamma_{SI} p_{rad}} \mathbf{c} s_\mu + \sqrt{p_{rad}} \mathbf{g} s_\mu + \mathbf{n} \right), \end{aligned} \tag{32}$$

where $\left| \mathbf{w}_k \hat{\mathbf{h}}_k \right| = 1$ and $\left| \mathbf{w}_k \hat{\mathbf{h}}_i \right| = 0$ when $M \gg K$ in massive MIMO systems [36]. In turn, the average power of the received signal $\hat{x}_k$ is given by (33), where Γ_{sig}, Γ_{in}, and Γ_n denote the power of the desired communication signal, the power of inter-user interference, and the sum power of the residual SI, radar interference and noise, respectively. The analytical expression of the desired signal power Γ_{sig} is derived as

$$\mathbb{E}\left[|\hat{x}_k|^2\right] = \underbrace{\frac{p_u}{1-\xi}\mathbb{E}\left[|1-\mathbf{w}_k\mathbf{e}_k|^2\right]}_{\Gamma_{sig}} + \underbrace{\sum_{i=1,i\neq k}^{K}\frac{p_u}{1-\xi}\mathbb{E}\left[|-\mathbf{w}_k\mathbf{e}_i|^2\right]}_{\Gamma_{in}} + \underbrace{\gamma_{SI}p_{rad}\mathbb{E}\left[|\mathbf{w}_k\mathbf{c}|^2\right] + p_{rad}\mathbb{E}\left[|\mathbf{w}_k\mathbf{g}|^2\right] + \mathbb{E}\left[|\mathbf{w}_k\mathbf{n}|^2\right]}_{\Gamma_n} \quad (33)$$

$$\begin{aligned}\Gamma_{sig} &= \frac{p_u}{1-\xi}\mathbb{E}\left[|1-\mathbf{w}_k\mathbf{e}_k|^2\right] \\ &\approx \frac{p_u}{1-\xi}\left((1-\xi)^2 + \frac{\xi}{M-K}\right), \end{aligned} \quad (34)$$

as $\mathbb{E}\left[|e_{m,k}|^2\right] = \xi\beta_k$ and $\mathbb{E}\left[\|\mathbf{w}_k\|^2\right] = \frac{1}{(M-K)\beta_k}$ [36].

Proof: See Appendix. ∎

Since $\mathbf{w}_k$ and $\mathbf{e}_i$ are mutually independent complex vectors, the power of the interference from other users is derived as

$$\begin{aligned}\Gamma_{in} &= \sum_{i=1,i\neq k}^{K}\frac{p_u}{1-\xi}\mathbb{E}\left[|-\mathbf{w}_k\mathbf{e}_i|^2\right] \\ &= \sum_{i=1,i\neq k}^{K}\frac{p_u}{1-\xi}\mathbb{E}\left[\|\mathbf{w}_k\|^2\right]\mathbb{E}\left[|e_{m,i}|^2\right] \\ &= \frac{p_u}{1-\xi}\mathbb{E}\left[\|\mathbf{w}_k\|^2\right]\sum_{i=1,i\neq k}^{K}\mathbb{E}\left[|e_{m,i}|^2\right] \\ &= \frac{p_u\xi}{(1-\xi)(M-K)\beta_k}\sum_{i=1,i\neq k}^{K}\beta_i. \end{aligned} \quad (35)$$

If $\beta_k = \beta_i$, $\forall k, i \in \{1,\ldots,K\}$, then Γ_{in} simplifies to

$$\Gamma_{in} = \frac{(K-1)p_u\xi}{(1-\xi)(M-K)}. \quad (36)$$

As for Γ_n, and assuming that $\mathbf{w}_k$ is independent of $\mathbf{c}$, $\mathbf{g}$ and $\mathbf{n}$, the power of residual SI—after ZF—is derived as

$$\mathbb{E}\left[|\mathbf{w}_k\mathbf{c}|^2\right] = \mathbb{E}\left[\|\mathbf{w}_k\|^2\right]\mathbb{E}\left[|c_m|^2\right] = \frac{p_{rad}\Lambda_m\gamma_{SI}}{(M-K)\beta_k}, \quad (37)$$

where Λ_m and γ_{SI} were defined as antenna isolation and SI suppression is subsections II-D and III-A, respectively. Now, the power of the radar interference is derived as

$$\mathbb{E}\left[|\mathbf{w}_k\mathbf{g}|^2\right] = \mathbb{E}\left[\|\mathbf{w}_k\|^2\right]\mathbb{E}\left[|g_m|^2\right] = \frac{p_{rad}\sum_{u=1}^{U}a_{u,m}^2}{(M-K)\beta_k}, \quad (38)$$

where $a_{u,m}$ is the channel gain of the radar return from the uth target, as given by (5). Additionally,

$$\mathbb{E}\left[|\mathbf{w}_k\mathbf{n}|^2\right] = \mathbb{E}\left[\|\mathbf{w}_k\|^2\right]\mathbb{E}\left[|n_m|^2\right] = \frac{\sigma_n^2}{(M-K)\beta_k}. \quad (39)$$

Thus, the sum power of SI, radar interference and noise is determined as

$$\Gamma_n = \frac{1}{(M-K)\beta_k}\left(p_{rad}\Lambda_m\gamma_{SI} + p_{rad}\sum_{u=1}^{U}a_{u,m}^2 + \sigma_n^2\right). \quad (40)$$

Based on the all the above, the SINR of the kth UE is obtained as (41). Now, when the BS has the perfect CSI (i.e. $\xi = 0$), this SINR expression can be simplified as

$$\psi_k^{ZF} = \frac{p_u\beta_k(M-K)}{p_{rad}\Lambda_m\gamma_{SI} + p_{rad}\sum_{u=1}^{U}a_{u,m}^2 + \sigma_n^2}. \quad (42)$$

In comparison to the ZF receiver, the ZF-OSIC receiver enjoys a massive MIMO gain of [37]

$$\|\mathbf{w}_k\|^2 = \frac{1}{\beta_k(M-(K-k+1))}. \quad (43)$$

Accordingly, the SINR of the signals received from the kth UE with ZF-OSIC is given by (44). If the BS has the perfect CSI, then $\psi_k^{ZF-OSIC}$ simplifies to

$$\psi_k^{ZF-OSIC} = \frac{p_u\beta_k(M-K+k-1)}{p_{rad}\Lambda_m\gamma_{SI} + p_{rad}\sum_{u=1}^{U}a_{u,m}^2 + \sigma_n^2}. \quad (45)$$

In SINR expressions (41) and (44), it is observed that the residual SI and radar interference are treated as noise by the ZF and ZF-OSIC receivers and they are suppressed. Accordingly, the capacity of the network is given by

$$C_{ZF} = \log_2\left(1+\psi_k^{ZF}\right), \quad (46)$$

for the ZF receiver, and

$$C_{ZF-OSIC} = \log_2\left(1+\psi_k^{ZF-OSIC}\right) \quad (47)$$

for the ZF-OSIC receiver.

V. Numerical Results and Simulations

The parameters used in the RadCom simulations and analytical calculations are given in Table I[2]. Since the duration of the uplink frame is sufficient to transmit only 10 OFDM symbols, 40 uplink frames are combined for radar image processing. It should be noted that different values can be used for application-specific sensing and communication requirements. The analytical results are verified by simulations, which are averaged over 10^5 random network instances with UEs randomly located within 400 m communication range and a single target with 0 dBm^2 RCS within the radar range of 200 m. 16-PSK is used for modulation of the OFDM radar symbols while QAM modulation is used for communication symbols.

In the results, the following schemes have been defined for comparison. **ZF-OSIC Com** and **ZF Com**, which are used as benchmarks for massive MIMO communication without any radar interference, while **ZF-OSIC RadCom** and **ZF**

[2]The carrier frequency and OFDM frame structure are chosen as in our downlink massive MIMO RadCom study [14], which is to demonstrate the practicality of our RadCom system for sensing and communication in both downlink and uplink.

$$\psi_k^{ZF} = \frac{\frac{p_u}{1-\xi}\left(\frac{\xi}{M-K}+(1-\xi)^2\right)}{\frac{p_u\xi}{(1-\xi)(M-K)\beta_k}\sum_{i=1,i\neq k}^{K}\beta_i + \frac{1}{(M-K)\beta_k}\left(p_{rad}\Lambda_m\gamma_{SI}+p_{rad}\sum_{u=1}^{U}a_{u,m}^2+\sigma_n^2\right)}$$
$$= \frac{p_u\beta_k\left(\xi+(M-K)\left(1-\xi\beta_k\right)^2\right)}{p_u\xi\sum_{i=1,i\neq k}^{K}\beta_i+(1-\xi)\left(p_{rad}\Lambda_m\gamma_{SI}+p_{rad}\sum_{u=1}^{U}a_{u,m}^2+\sigma_n^2\right)} \quad (41)$$

$$\psi_k^{ZF-OSIC} = \frac{p_u\beta_k\left(\xi+(M-K+k-1)\left(1-\xi\beta_k\right)^2\right)}{p_u\xi\sum_{i=1,i\neq k}^{K}\beta_i+(1-\xi)\left(p_{rad}\Lambda_m\gamma_{SI}+p_{rad}\sum_{u=1}^{U}a_{u,m}^2+\sigma_n^2\right)} \quad (44)$$

TABLE I
UPLINK RADCOM SYSTEM PARAMETERS

Parameter	Value	Description
f_c	5.8 GHz	Carrier frequency
B	100 MHz	Bandwidth
Δf	114 kHz	Subcarrier Spacing
Δt	200 μs	TDD frame duration
T_{sym}	8.77 μs	Elementary symbol duration
T_{cp}	1.33 μs	Cyclic-prefix duration
T_o	10 μs	OFDM symbol duration
L	877	Number of OFDM subcarriers
N	40	Symbols in each radar waveform
T_{rad}	8 ms	Radar processing time ($L \times \Delta t$)
p_{N0}	-174 dBm/Hz	Noise spectral density
$G_P = 10\log_{10}NL$	55.45 dB	Radar processing gain

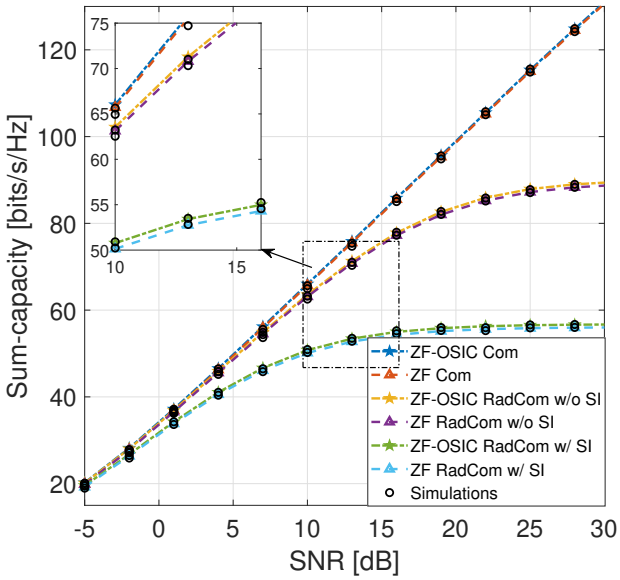

Fig. 3. Sum-capacity of the network as a function of communication SNR in the uplink RadCom with perfect CSI (i.e. $\xi = 0$) - $p_{rad} = p_{com}$, $M = 100$ BS antennas, and $K = 10$ UEs.

RadCom refer to the proposed RadCom schemes with ZF-OSIC and ZF receivers, respectively. Additionally, **w/ SI** indicates that residual SI exists after SI cancellation, while **w/o SI** indicates that SI is completely canceled by the SI canceler. Furthermore, the variance of imperfect CSI is indicated by ξ, and thus, $\xi = 0$ refers to the perfect CSI case.

Fig. 3 illustrates the sum-capacity of the RadCom network when the BS has the perfect CSI (i.e. $\xi = 0$) and $p_{rad} = p_{com}$. It is observed that that ZF-OSIC marginally outperforms the ZF in terms of sum-capacity. Moreover, completely cancelling the SI substantially improves the network capacity. While the capacity of ZF and ZF-OSIC without radar interference (i.e. **ZF-OSIC Com** and **ZF Com**) improve linearly with SNR, the capacity of the ZF RadCom and ZF-OSIC RadCom saturates at high SNR regions due to the radar interference; although it is significantly suppressed by the ZF or ZF-OSIC. This is because in the high SNR region, the noise power becomes very small compared to the signal power, and hence, the capacity is mainly limited by the interference. On the other hand, it is evident from Fig. 3 that the analytical capacity derivations coincide with the simulation results for all SNR values.

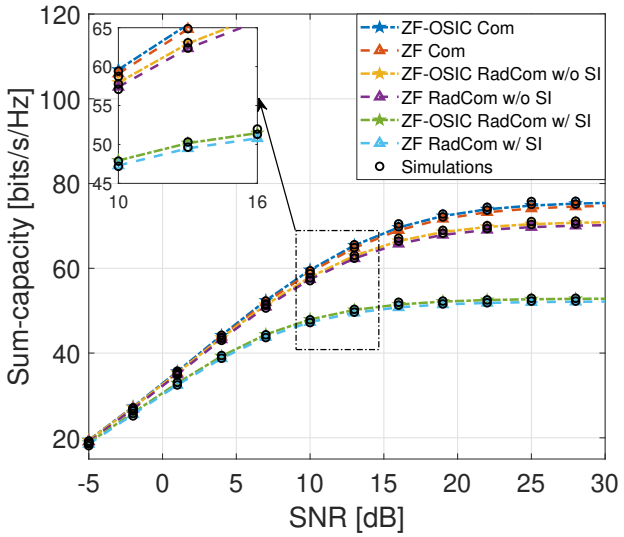

Fig. 4. Sum-capacity of the network as a function of communication SNR in the uplink RadCom with imperfect CSI and $\xi = 0.05$ - $p_{rad} = p_{com}$, $M = 100$ BS antennas, and $K = 10$ UEs.

In Fig. 4, the impact of imperfect CSI on the sum-capacity is investigated, where the BS is assumed to have imperfect CSI with $\xi = 0.05$ error variance. It is clear that the sum-capacity is degraded by the CSI errors compared to the perfect CSI case given in Fig 3. A more detailed comparison of the impact of imperfect CSI estimation on the sum-capacity is given in Fig. 5, where CSI estimation errors of variances $\xi = 0$, $\xi = 0.05$, and $\xi = 0.1$ are considered for the case when the SI is completely cancelled by the DSP canceller. It can be seen that CSI errors limit the capacity, especially at high SNR

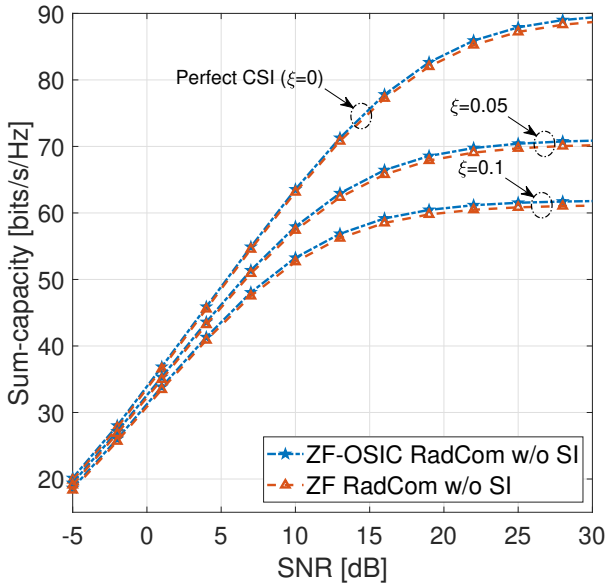

Fig. 5. Impact of channel estimation errors on the network sum-capacity in the uplink RadCom when SI is completely cancelled out with DSP canceller - $p_{rad} = p_{com}$, $M = 100$ BS antennas, and $K = 10$ UEs.

values. Evidently, ZF-OSIC still slightly outperforms ZF, even with imperfect CSI; however, its computational complexity is significantly higher due to its iterative operation for inter-user interference cancellation.

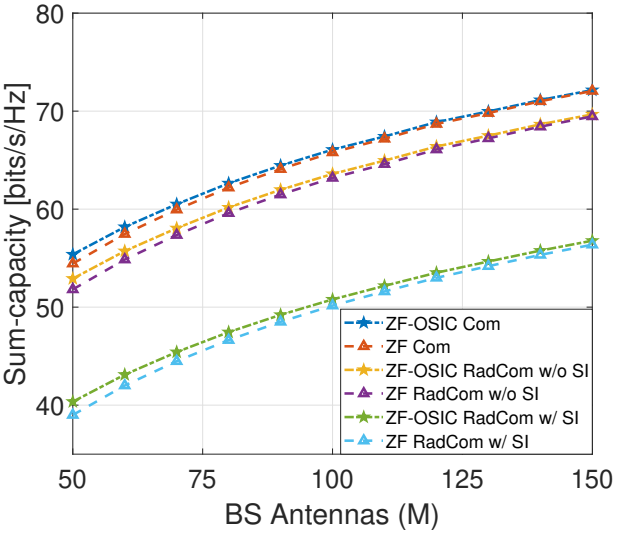

Fig. 6. Sum-capacity of uplink RadCom with various number of BS antennas. $p_{rad} = p_{com}$, $K = 10$ UEs, and SNR is 10 dB.

Fig. 6 illustrates the sum-capacity of the RadCom network as a function of the number of BS antennas M. Clearly, as M increases, the performance of ZF approaches that of ZF-OSIC, and this makes ZF more favorable with larger M, since its complexity is lower. When SI is cancelled, the sum-capacity of RadCom is only around 3 bits/s/Hz lower than the ZF capacity without radar interference. Residual SI may significantly degrade the sum-capacity, and thus, completely eliminating the SI is crucial for the maximization of the

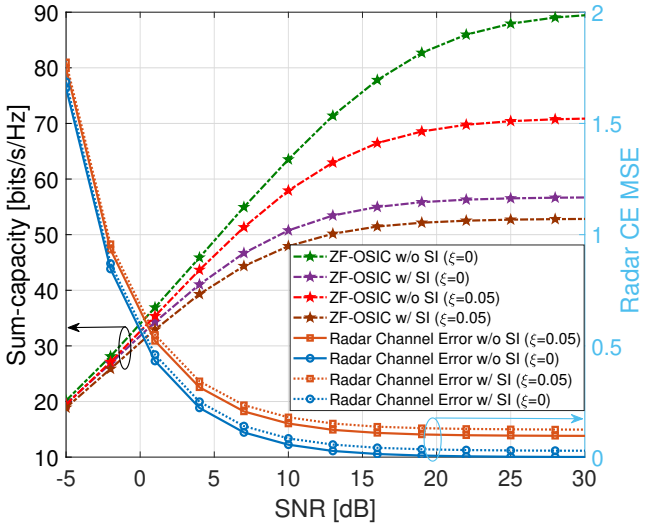

Fig. 7. Sum-capacity and radar channel estimation (CE) MSE as communication SNR increases within various network conditions - $p_{rad} = p_{com}$, $M = 100$ BS antennas, and $K = 10$ UEs.

RadCom sum-capacity performance.

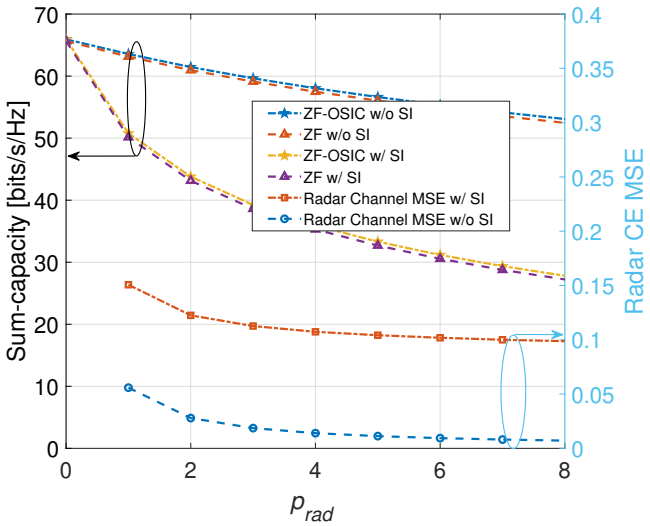

Fig. 8. Sum-capacity and radar channel estimation errors as a function of radar power output p_{rad} - $p_{com} = 1$ W, $M = 100$ BS antennas, $K = 10$ UEs, and communication SNR is 10 dB.

The radar detection performance is affected by the radar channel estimation (CE) and radar SINR obtained during the radar processing. Fig. 7 illustrates the sum-capacity and radar CE mean square error (MSE) as a function of the communication SNR, where it can be seen that the SI significantly degrades both of performance metrics. On the other hand, very low SNR values cause high symbol error rate, and thus, the radar MSE is excessively high in this region as the subtracted communication signals—to estimate the radar channel—have significantly more errors. Fig. 8 shows these two metrics as a function of the radar output power p_{rad} when the communication output power p_{com} is fixed, such that communication SNR is 10 dB. In this case, as the radar output power increases, the communication sum-capacity decreases

due to the radar interference. However, perfect SI cancellation mitigates this sum-capacity degradation as can be seen in the comparison between the sum-capacities with and without SI. Moreover, perfect SI cancellation also improves the radar CE accuracy. This reveals that the main problem in a short-range RadCom system is the SI, which is caused by simultaneously operating the transmit and receive antennas. An excellent RF and antenna isolation between the radar transmit antennas and antenna array elements along with a decent baseband digital SI canceller will therefore maximize the performance of the RadCom system in terms of communication sum-capacity and radar detection.

Radar image SINR is the main factor that determines the detection accuracy of the targets in OFDM radars [38]. In the uplink radar sensing, the radar SINR is calculated as a ratio of the received power of the radar returns to the power of the noise and residual communication signals[3]. Fig. 9 illustrates the sum-capacity and radar image SINR, which includes the radar processing gain while the radar output power p_{rad} increases. When $p_{rad} = 1$ W, the radar SINR reaches around 25 dB and when $p_{rad} = 2$ W, it reaches around 28 dB with perfect CSI. On the other hand, the communication sum-capacity with the residual SI is severely affected by the increase in the radar output power. However, when the residual SI is completely canceled, the sum-capacity drop caused by the radar output is less severe. As would be expected, the imperfect CSI degrades the radar image SINR as well as the communication sum-capacity, since CSI errors cause more residual communication signals in the acquired radar signals.

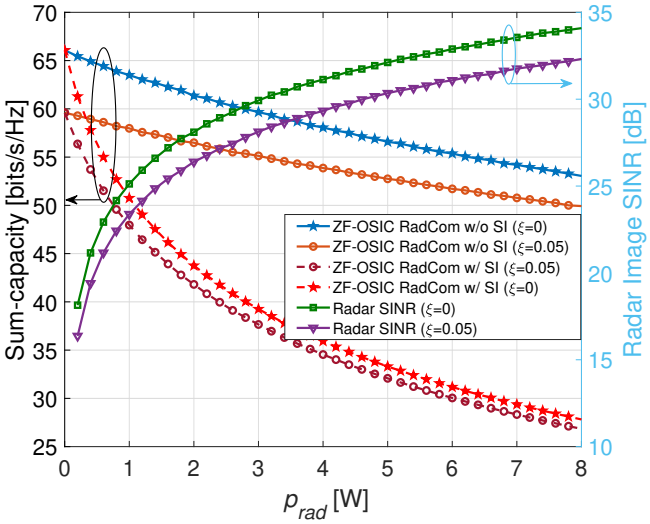

Fig. 9. Sum-capacity and radar image SINR after OFDM radar processing as a function of radar output power p_{rad}, p_{com}=1 W, $M = 100$ BS antennas, $K = 10$ UEs, and communication SNR is 10 dB.

To give an insightful and meaningful comparison between various radar image SINR values, the obtained radar images by symbol-based OFDM radar processing are presented in Figs. 10 and 11, which compare the cases where the residual SI is present, and completely canceled, respectively. Two targets with 0 dBm^2 RCS are present in the radar range, which are located 90 m and 140m away from the BS. Their velocities are 15 m/s and -10 m/s, respectively. Fig. 10 illustrates the radar image which has 12 dB SINR. In this figure, the closer target may be identified; however, the second target is nearly impossible to recognize due to the high noise and interference. Moreover, it can be seen that in Fig. 10a that the visibility of the target is reduced by the SI while the target can be estimated easier when the SI is removed, as shown in Fig. 10b. Fig 11 presents the radar images with 17 dB radar image SINR, where it is evident that radar images are significantly enhanced compared to Fig. 10, which is due to the higher radar SINR. Targets can be clearly seen especially when the SI is eliminated. Taking into account the radar image SINR and communication capacity trade-off given in Fig. 9, one can observe that a relatively low radar output power (e.g. $p_{rad} = 1$ W) is sufficient to obtain a clear radar image, while the communication sum-capacity is dropped only by about 3 bits/s/Hz in this specific radar and communication network setup.

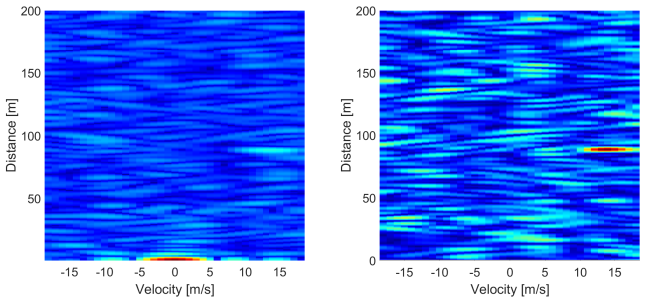

Fig. 10. Radar images of two targets with (a) SI and (b) after SI cancellation. Radar image SINR after radar processing is 12 dB.

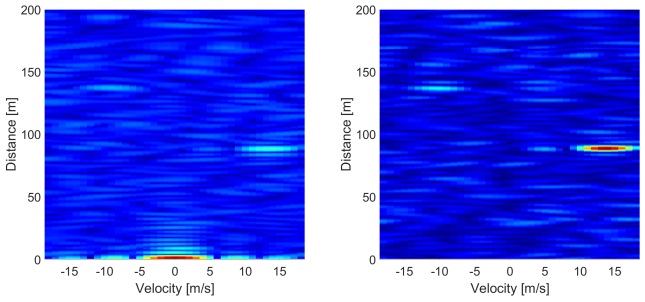

Fig. 11. Radar images of two targets with (a) SI and (b) after SI cancellation. Radar image SINR after radar processing is 17 dB.

VI. Conclusions

In this study, a joint uplink communication and OFDM radar sensing architecture using large-scale antenna arrays is proposed. The ZF and ZF-OSIC receivers are used to eliminate the inter-user interference and radar interference while detecting the UEs' data. Thereafter, the detected UEs' data are canceled from the received signals to acquire the radar

[3]Note that the power of the residual SI is not included in this calculation, since the SI can be recognized in the radar image as an object that is very close to the radar, and hence, it can be entirely removed. Consequently, the residual SI mainly degrades the communication sum-capacity performance.

returns. Then, the symbol-based OFDM radar processing is applied to identify the target parameters. A trade-off between the radar detection and communication sum-capacity has been observed with regards to the radar power output. However, especially in short-range radar applications, a low radar output power is sufficient to detect the targets, and hence, it is possible to effectively perform both uplink communication and radar sensing using the same platform in the same time-frequency resources. Analytical capacity expressions of the uplink have been derived and verified via simulations under perfect and imperfect CSI scenarios. The main problem in short-range RadCom systems has been identified as self-interference, while demonstrating that entirely removing it from the received signals maximizes the network sum-capacity and improves the radar target detection performance.

APPENDIX

The analytical expression of $\mathbb{E}\left[\left|1-\mathbf{w}_k\mathbf{e}_k\right|^2\right]$ is derived as

$$\begin{aligned}
&\mathbb{E}\left[\left|1-\mathbf{w}_k\mathbf{e}_k\right|^2\right] \\
&= \mathbb{E}\left[\left[1-\Re\left(\mathbf{w}_k\mathbf{e}_k\right)\right]^2+\left[\Im\left(\mathbf{w}_k\mathbf{e}_k\right)\right]^2\right] \\
&= 1-2\mathbb{E}\left[\Re\left(\mathbf{w}_k\mathbf{e}_k\right)\right]+\mathbb{E}\left[\left(\Re\left(\mathbf{w}_k\mathbf{e}_k\right)\right)^2+\left(\Im\left(\mathbf{w}_k\mathbf{e}_k\right)\right)^2\right] \\
&= 1-2\mathbb{E}\left[\Re\left(\mathbf{w}_k\mathbf{e}_k\right)\right]+\mathbb{E}\left[\left|\mathbf{w}_k\mathbf{e}_k\right|^2\right] \\
&\approx 1-2\mathbb{E}\left[\left|\mathbf{w}_k\mathbf{e}_k\right|\right]+\mathbb{E}\left[\left|\mathbf{w}_k\mathbf{e}_k\right|^2\right] \\
&\approx 1-2\xi+\xi^2+\frac{\xi}{M-K} \\
&\approx (1-\xi)^2+\frac{\xi}{M-K},
\end{aligned} \tag{48}$$

which is based on $\mathbf{w}_k$ and $\mathbf{e}_k$ being mutually independent random vectors, and thus $\mathbb{E}\left[\Re\left(\mathbf{w}_k\mathbf{e}_k\right)\right] \approx \mathbb{E}\left[\left|\mathbf{w}_k\mathbf{e}_k\right|\right]$, $\mathbb{E}\left[\left|\mathbf{w}_k\mathbf{e}_k\right|\right] \approx \xi$, and $\mathbb{E}\left[\left|\mathbf{w}_k\mathbf{e}_k\right|^2\right] \approx \xi^2+\frac{\xi}{(M-K)}$ [14].

REFERENCES

[1] A. Sultan and M. Pope, *Digital cellular telecommunications system (Phase 2+) (GSM); Universal Mobile Telecommunications System (UMTS); LTE; 5G; Release 15, 3GPP TR 21.915 version 15.0.0 Release 15*. 2020.

[2] S. Henry, A. Alsohaily, and E. S. Sousa, "5G is real: Evaluating the compliance of the 3GPP 5G new radio system with the ITU IMT-2020 requirements," *IEEE Access*, vol. 8, pp. 42828–42840, 2020.

[3] P. Kumari, J. Choi, N. Gonzalez-Prelcic, and R. W. Heath, "IEEE 802.11ad-based radar: An approach to joint vehicular communication-radar system," *IEEE Trans. Veh. Technol.*, vol. 67, no. 4, pp. 3012–3027, 2018.

[4] R. S. Thoma, C. Andrich, G. D. Galdo, M. Dobereiner, M. A. Hein, M. Kaske, G. Schafer, S. Schieler, C. Schneider, A. Schwind, and P. Wendland, "Cooperative passive coherent location: A promising 5G service to support road safety," *IEEE Commun. Mag.*, vol. 57, pp. 86–92, Sep. 2019.

[5] B. Nuss, L. Sit, M. Fennel, J. Mayer, T. Mahler, and T. Zwick, "MIMO OFDM radar system for drone detection," *Proc. 18th International Radar Symposium (IRS)*, pp. 1–9, 2017.

[6] Y. Kwag, I. Woo, H. Kwak, and Y. Jung, "Multi-mode SDR radar platform for small air-vehicle drone detection," in *2016 CIE International Conference on Radar (RADAR)*, pp. 1–4, Oct 2016.

[7] D. Solomitckii, M. Gapeyenko, V. Semkin, S. Andreev, and Y. Koucheryavy, "Technologies for efficient amateur drone detection in 5G millimeter-wave cellular infrastructure," *IEEE Commun. Mag.*, vol. 56, pp. 43–50, Jan 2018.

[8] N. Jayaweera, D. Marasinghe, N. Rajatheva, and M. Latva-Aho, "Factory automation: Resource allocation of an elevated LiDAR system with URLLC requirements," in *2020 2nd 6G Wireless Summit (6G SUMMIT)*, pp. 1–5, March 2020.

[9] F. Liu, C. Masouros, A. P. Petropulu, H. Griffiths, and L. Hanzo, "Joint radar and communication design: Applications, state-of-the-art, and the road ahead," *IEEE Trans. Commun.*, vol. 68, pp. 3834–3862, June 2020.

[10] D. Ma, N. Shlezinger, T. Huang, Y. Liu, and Y. C. Eldar, "Joint radar-communication strategies for autonomous vehicles: Combining two key automotive technologies," *IEEE Signal Process. Mag.*, vol. 37, pp. 85–97, July 2020.

[11] S. Zhang, H. Zhang, and L. Song, "Beyond D2D: Full dimension UAV-to-everything communications in 6G," *IEEE Trans. Veh. Technol.*, vol. 69, pp. 6592–6602, June 2020.

[12] W. Saad, M. Bennis, and M. Chen, "A vision of 6G wireless systems: Applications, trends, technologies, and open research problems," *IEEE Netw.*, vol. 34, pp. 134–142, May 2020.

[13] A. Hassanien, M. G. Amin, E. Aboutanios, and B. Himed, "Dual-function radar communication systems: A solution to the spectrum congestion problem," *IEEE Signal Process. Mag.*, vol. 36, pp. 115–126, Sep. 2019.

[14] M. Temiz, E. Alsusa, and M. W. Baidas, "A dual-functional massive MIMO OFDM communication and radar transmitter architecture," *IEEE Trans. Veh. Technol.*, vol. 69, pp. 14974–14988, Dec. 2020.

[15] B. Li and A. P. Petropulu, "Joint transmit designs for coexistence of MIMO wireless communications and sparse sensing radars in clutter," *IEEE Trans. Aerosp. Electron. Syst.*, vol. 53, pp. 2846–2864, Dec 2017.

[16] F. Liu, C. Masouros, A. Li, H. Sun, and L. Hanzo, "MU-MIMO communications with MIMO radar: From co-existence to joint transmission," *IEEE Trans. Wireless Commun.*, vol. 17, pp. 2755–2770, April 2018.

[17] B. Paul, A. R. Chiriyath, and D. W. Bliss, "Survey of RF communications and sensing convergence research," *IEEE Access*, vol. 5, pp. 252–270, 2017.

[18] Q. Li, K. Dai, Y. Zhang, and H. Zhang, "Integrated waveform for a joint radar-communication system with high-speed transmission," *IEEE Wireless Commun. Lett.*, vol. 8, no. 4, pp. 1208–1211, 2019.

[19] C. Shi, F. Wang, S. Salous, and J. Zhou, "Joint subcarrier assignment and power allocation strategy for integrated radar and communications system based on power minimization," *IEEE Sensors J.*, vol. 19, no. 23, pp. 11167–11179, 2019.

[20] J. A. Zhang, X. Huang, Y. J. Guo, J. Yuan, and R. W. Heath, "Multibeam for joint communication and radar sensing using steerable analog antenna arrays," *IEEE Trans. Veh. Technol.*, vol. 68, pp. 671–685, Jan 2019.

[21] M. L. Rahman, J. A. Zhang, X. Huang, Y. J. Guo, and R. W. Heath, "Framework for a perceptive mobile network using joint communication and radar sensing," *IEEE Trans. Aerosp. Electron. Syst.*, vol. 56, pp. 1926–1941, June 2020.

[22] C. D'Andrea, S. Buzzi, and M. Lops, "Communications and radar coexistence in the massive MIMO regime: Uplink analysis," *IEEE Trans. Wireless Commun.*, vol. 19, pp. 19–33, Jan 2020.

[23] C. Sturm, Y. L. Sit, M. Braun, and T. Zwick, "Spectrally interleaved multi-carrier signals for radar network applications and multi-input multi-output radar," *IET Radar, Sonar Navig.*, vol. 7, pp. 261–269, March 2013.

[24] S. Sun, T. S. Rappaport, T. A. Thomas, A. Ghosh, H. C. Nguyen, I. Z. Kovacs, I. Rodriguez, O. Koymen, and A. Partyka, "Investigation of prediction accuracy, sensitivity, and parameter stability of large-scale propagation path loss models for 5G wireless communications," *IEEE Trans. Veh. Technol.*, vol. 65, no. 5, pp. 2843–2860, 2016.

[25] M. Temiz, E. Alsusa, and L. Danoon, "Impact of imperfect channel estimation and antenna correlation on quantised massive multiple-input multiple-output systems," *IET Commun.*, vol. 13, no. 9, pp. 1262–1270, 2019.

[26] P. Aquilina and T. Ratnarajah, "Performance analysis of IA techniques in the MIMO IBC with imperfect CSI," *IEEE Trans. Commun.*, vol. 63, pp. 1259–1270, April 2015.

[27] Y. L. Sit, B. Nuss, and T. Zwick, "On mutual interference cancellation in a MIMO OFDM multiuser radar-communication network," *IEEE Trans. on Veh. Technol.*, vol. 67, pp. 3339–3348, April 2018.

[28] M. A. Richards, J. A. Scheer, and W. A. Holm, eds., *Principles of Modern Radar: Basic principles*. Institution of Engineering and Technology, 2010.

[29] M. Heino, D. Korpi, T. Huusari, E. Antonio-Rodriguez, S. Venkatasubramanian, T. Riihonen, L. Anttila, C. Icheln, K. Haneda, R. Wichman, and M. Valkama, "Recent advances in antenna design and interference cancellation algorithms for in-band full duplex relays," *IEEE Commun. Mag.*, vol. 53, pp. 91–101, May 2015.

[30] T. Snow, C. Fulton, and W. J. Chappell, "Transmit-receive duplexing using digital beamforming system to cancel self-interference," *IEEE Trans. Microw. Theory Techn.*, vol. 59, pp. 3494–3503, Dec 2011.

[31] X. Chen, S. Zhang, and Q. Li, "A review of mutual coupling in MIMO systems," *IEEE Access*, vol. 6, pp. 24706–24719, 2018.

[32] K. Alexandris, A. Balatsoukas-Stimming, and A. Burg, "Measurement-based characterization of residual self-interference on a full-duplex MIMO testbed," *Proc. IEEE 8th Sensor Array and Multichannel Signal Processing Workshop (SAM)*, pp. 329–332, 2014.

[33] F. J. Soriano-Irigaray, J. S. Fernandez-Prat, F. J. Lopez-Martinez, E. Martos-Naya, O. Cobos-Morales, and J. T. Entrambasaguas, "Adaptive self-interference cancellation for full duplex radio: Analytical model and experimental validation," *IEEE Access*, vol. 6, pp. 65018–65026, 2018.

[34] C. Baquero Barneto, T. Riihonen, M. Turunen, L. Anttila, M. Fleischer, K. Stadius, J. Ryynanen, and M. Valkama, "Full-duplex OFDM radar with LTE and 5G NR waveforms: Challenges, solutions, and measurements," *IEEE Trans. Microw. Theory Techn.*, vol. 67, pp. 4042–4054, Oct 2019.

[35] M. A. Albreem, M. Juntti, and S. Shahabuddin, "Massive MIMO detection techniques: A survey," *IEEE Commun. Surveys Tuts.*, vol. 21, pp. 3109–3132, Fourthquarter 2019.

[36] H. Q. Ngo, E. G. Larsson, and T. L. Marzetta, "Energy and spectral efficiency of very large multiuser MIMO systems," *IEEE Trans. Commun.*, vol. 61, no. 4, pp. 1436–1449, 2013.

[37] T. Liu, J. Tong, Q. Guo, J. Xi, Y. Yu, and Z. Xiao, "Energy efficiency of massive MIMO systems with low-resolution ADCs and successive interference cancellation," *IEEE Trans. Wireless Commun.*, vol. 18, pp. 3987–4002, Aug 2019.

[38] C. Sturm and W. Wiesbeck, "Waveform design and signal processing aspects for fusion of wireless communications and radar sensing," *Proc. IEEE*, vol. 99, pp. 1236–1259, July 2011.